Manuscript submitted to *Security and Safety*, For Peer Review Only, Vol. x, xxxxxxx (2023)
https://doi.org/10.1051/sands/xxxxxxx
sands.edpsciences.org

Research Article OPEN ACCESS

Section Category

Distributed Control of Multiarea Power Systems with Virtual Power Plants under DoS Attacks and Actuator Failures

Yichao Wang[1] and Zhi-Wei Liu[1*]

[1] *School of Artificial Intelligence and Automation, Wuhan 430074, China*

Received: xx xxxxx 2022 / Revised: xx xxxxx 2022 / Accepted: xx xxxxx 2022 / Published online: xx xxxxx 2022

Abstract This paper focuses on the distributed control issue of multi-area power systems integrated with virtual power plants (VPPs) under the coexistence scenario of denial-of-service (DoS) attacks and actuator failures. A distributed control strategy is developed by leveraging local and neighboring measurements, which guarantees the desired operational performance of the system. Based on the Lyapunov stability theory, sufficient condition for ensuring the system stability is derived. Furthermore, the linear matrix inequality (LMI) technique is employed to solve the controller gain parameters. Finally, the validity and feasibility of the proposed control strategy are verified via simulation experiments on a two-area power system integrated with VPPs.

Keywords Load frequency control (LFC), denial of service (DoS) attacks, actuator failures, virtual power plants (VPPs)

Citation Yichao Wang, Zhi-Wei Liu. Distributed Control of Multiarea Power Systems with Virtual Power Plants under DoS Attacks and Actuator Failures. Security and Safety 2023; **x**: xxxxxxx. https://doi.org/10.1051/sands/xxxxxxx

1 Introduction

Power systems are critical infrastructures supporting modern society, where frequency stability stands as the most fundamental operational necessity. Within large-scale interconnected power systems, the system is commonly partitioned into multiple control areas to facilitate operation and coordination, and load frequency control (LFC) is employed to regulate frequency deviations and inter-area power exchanges by balancing generation and demand in real time [1, 2]. With the continuous growth of system scale and power demand, the large-scale integration of renewable and distributed energy resources (DERs) fundamentally alters system inertia and regulation characteristics, causing traditional generation-dominated LFC frameworks to face increasing challenges in terms of flexibility and dynamic response capability.

In recent years, virtual power plants (VPPs) have emerged as an effective paradigm for aggregating large-scale DERs, including wind power, electric vehicles, and energy storage systems, into a coordinated and dispatchable entity [3]. By facilitating the participation of these heterogeneous resources in ancillary services, VPPs introduce fast and flexible regulation capabilities into LFC of multi-area power systems [4–9]. However, such flexibility is achieved at the cost of increased reliance on communication networks and distributed control architectures, which tightens the coupling between cyber information layers and physical system dynamics. Consequently, frequency regulation becomes more vulnerable to non-ideal operating conditions, such as cyber-attacks and actuator failure.

Among various threats to cyber-physical power systems, denial-of-service (DoS) attacks and actuator failures represent two typical yet fundamentally different sources of vulnerability in VPP-integrated LFC systems. DoS attacks disrupt the availability of measurement and control signals by blocking or delaying

* Corresponding author (email: zwliu@hust.edu.cn)

communication channels, thereby preventing controllers from obtaining timely system information or delivering effective control commands [10–17]. In contrast, actuator failure degrade the physical execution of control actions due to mechanical wear, electrical malfunctions, or environmental disturbances, leading to discrepancies between intended control inputs and actual system responses [18–24]. When these two types of abnormal conditions coexist, their impacts simultaneously affect the information transmission layer and the control execution layer, resulting in compounded uncertainties and significantly increased challenges for stability analysis and controller design in multi-area power systems.

Existing studies have extensively investigated LFC problems in power systems from different perspectives. With the increasing integration of communication networks, a substantial body of research has focused on enhancing the resilience of LFC against cyber threats, particularly denial-of-service (DoS) attacks. Distributed and resilient control strategies have been proposed to tolerate intermittent communication interruptions, packet losses, or delayed information exchange, and stability or performance guarantees have been established under various DoS attack models [12–17]. These works provide valuable insights into protecting frequency regulation against information-layer disruptions, but typically assume that control execution remains reliable.

In parallel, actuator failures and component degradations have been widely studied investigated within the framework of fault-tolerant control. Existing approaches address partial or complete loss of actuator effectiveness through reconfiguration, compensation, or adaptive mechanisms, thereby maintaining acceptable LFC performance under degraded physical actuation [18–24]. However, these studies usually presume normal communication conditions and do not explicitly consider adversarial disturbances in the cyber layer.

More recently, several studies have incorporated distributed energy resources and virtual power plants into LFC frameworks, highlighting their potential to enhance flexibility and regulation speed in multi-area power systems [4–9]. Despite these advances, most existing VPP-based LFC schemes are developed under idealized assumptions, such as reliable communication and fault-free actuation, or rely on simplified inter-area coupling models that neglect the simultaneous influence of cyber and physical anomalies [27]. As a consequence, the current literature fails to adequately address the concurrent existence of DoS attacks and actuator failures in VPP-integrated multi-area power systems.

Motivated by the above observations, this paper studies the distributed LFC problem for VPP-integrated multi-area power systems under the coexistence of DoS attacks and actuator failures. Unlike existing resilient LFC studies that primarily address cyber attacks such as DoS while assuming normal actuator operation [12–17], and fault-tolerant control approaches that focus on actuator failures under reliable communication conditions [18–24], this work explicitly considers the simultaneous presence of both types of abnormalities. A unified system modeling framework is established to distinguish and capture their fundamentally different impacts on information transmission and control execution. Furthermore, in contrast to existing studies that neglect inter-area coupling dynamics or adopt simplified decoupled representations [25, 30, 27], inter-area interactions are explicitly incorporated to reflect practical multi-area operating conditions. Based on this framework, a distributed coordinated control strategy relying on local and neighboring measurements is developed. Sufficient criteria are established to ensure bounded stability of the closed-loop system under such coupled cyber-physical uncertainties, and the controller gains are obtained via linear matrix inequality (LMI) techniques. A VPP-integrated two-area power system model is adopted for simulation verification, which testifies to the efficacy and robustness of the method developed in this paper.

The organization of the subsequent sections is presented as follows. The system modeling and problem formulation are addressed in Section 2. The stability analysis and the controller design procedure are elaborated in Section 3. Section 4 illustrates the simulation results and verifies the effectiveness of the proposed method. Finally, the conclusion is given in Section 5.

2 System Modeling and Problem Formulation

In this section, we first present the model of the multi-area power system constituting the VPPs. Considering that practical power systems are susceptible to adverse disturbances, such as DoS attacks and actuator failures, corresponding models are developed to characterize these effects. Furthermore, an

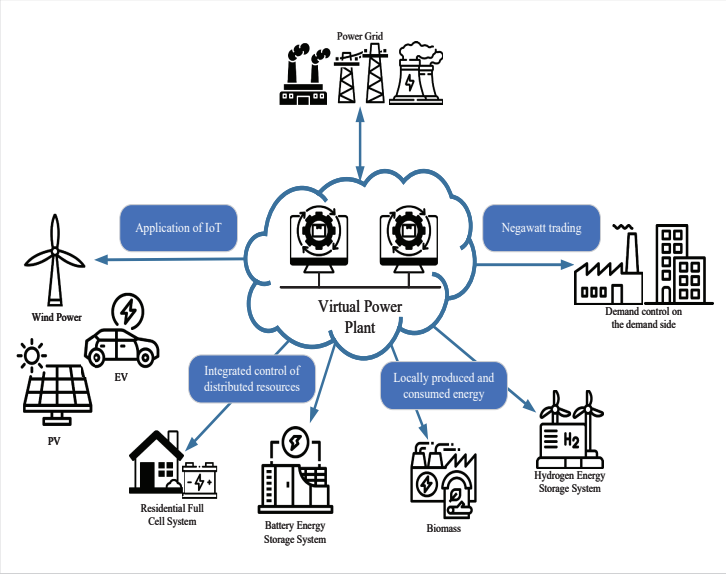

Figure 1. General structure of VPPs.

integrated system model that incorporates these factors is established to facilitate subsequent systematic analysis of their impact on system performance.

2.1 Modeling VPPs

As illustrated in Fig. 1, a VPP can be interpreted as an aggregation of heterogeneous distributed energy resources (DERs), which enables it to participate in grid scheduling as a unified entity. In this study, VPPs consisting of wind power generation, energy storage systems (ESSs), and electric vehicles (EVs) are considered, where these components collaboratively provide frequency regulation services to the power grid.

2.1.1 Wind power Model

In this paper, we adopt the aerodynamic model of wind power generation described in [28]. For a given wind speed and with the tip-speed ratio held at its optimal level, the regulation of the wind turbine's output power can be achieved through pitch angle opening adjustment. To analyze the LFC problem, the dynamics of wind power generation are characterized by a first-order model.

$$\Delta P_{\text{wind}} = \Delta\beta \cdot G_{wind} = \Delta\beta \cdot \frac{k_\beta}{1 + T_{wind}s} \tag{1}$$

where $\Delta\beta$ denotes the angular variation of the blade pitch angle, G_{wind} represents the power transfer function of the wind turbine, T_{wind} stands for the response time of the wind turbine, and k_β indicates the pitch angle control slope.

2.1.2 Electric vehicles Model

As mobile energy storage units, EVs can flexibly participate in frequency and voltage regulation of the power grid through controlled charging and discharging processes. The large-scale integration of EVs therefore plays a significant role in maintaining the stable operation of power systems. Assuming that the number of EVs remains constant, this paper establishes the following model for EV-based frequency regulation:

$$\Delta P_{ev} = \Delta U_{ev} \cdot G_{ev} = \Delta U_{ev} \cdot \frac{1}{1 + T_{ev}s} \tag{2}$$

where ΔU_{ev} denotes the charge-discharge depth of the electric vehicle battery, and T_{ev} represents the response time of the electric vehicle system.

2.1.3 Energy Storage Systems Model

During power system frequency regulation, energy storage systems (ESSs) can serve as highly efficient ancillary resources, enhancing the dynamic response to frequency deviations while alleviating the transient regulation burden on thermal power units. Considering the inherent response delay associated with ESS charging and discharging processes, a first-order lag model is adopted in this paper to characterize their dynamic behavior within the load frequency control (LFC) framework of hybrid power systems. The corresponding model is given as follows:

$$\Delta P_{ess} = \Delta P_s \cdot G_{ess} = \Delta P_s \cdot \frac{1}{1 + T_{ess} s} \tag{3}$$

where ΔP_s refers to the energy storage instantaneous power, while G_{ess} and T_{ess} correspond to the transfer function and response time of the energy storage system, respectively.

2.2 Modeling of Multi-Area Power Systems Integrated with VPPs

By responding to Automatic Generation Control (AGC) signals, VPPs take part in LFC, which in turn supports system frequency regulation. The power system investigated in this paper is assumed to consist of N interconnected areas linked by tie-lines. From the perspective of LFC modeling, the dynamics of the i-th area include frequency deviation, tie-line power exchange, turbine–governor dynamics, and the ACE-based feedback mechanism. According to [28], the mathematical representation of the i-th area is given as follows:

$$\begin{cases} \Delta f_i(s) = \frac{1}{D_i + sM_i} \Delta P(s) \\ \Delta P_{tie-i}(s) = \frac{2\pi}{s} \sum\limits_{j=1, j\neq i}^{N} T_{ij} \left(\Delta f_i(s) - \Delta f_j(s) \right) \\ \Delta P_{mi}(s) = \frac{1}{1+sT_{chi}} \Delta P_{vi}(s) \\ \Delta P_{vi}(s) = \frac{1}{1+sT_{gi}} \left(u_i(s) - \frac{1}{R_i} \Delta f_i(s) \right) \\ ACE_i(s) = \beta_i \Delta f_i(s) + \Delta P_{tie-i}(s) \end{cases} \tag{4}$$

where $\Delta P(s) = (\Delta P_{mi}(s) + \Delta P_{windi}(s) + \Delta P_{essi}(s) + \Delta P_{evi}(s) - \Delta P_{di}(s) - \Delta P_{tie-i}(s))$.

Remark 1. *In Eq. (4), the first equation describes the frequency dynamics, the second captures the tie-line power interactions among interconnected areas, the third and fourth represent the turbine–governor dynamics, and ACE_i denotes the area control error, which serves as the key feedback signal in LFC.*

Remark 2. *In this study, small communication delays are neglected as they are orders of magnitude smaller than the system's sampling period. This simplification is justified by the integration of high-performance communication infrastructures (e.g., 5G and TSN) in modern VPPs, which ensure ultra-low delay [29]. Furthermore, relevant studies in the existing literature have also not considered the impact of communication delays on the research problem [28, 30, 31].*

The state-space representation corresponding to the i-th area is given by

$$\begin{cases} \dot{x}_i(t) = A_{ii} x_i(t) + B_i u_i(t) + F_i w_i(t) + \sum\limits_{j=1, j\neq i}^{n} A_{ij} x_j(t) \\ y_i(t) = C_i x_i(t) \end{cases} \tag{5}$$

where $x_i(t) = col\left\{\Delta f_i(t), \Delta P_{tie-i}(t), \Delta P_{mi}(t), \Delta P_{vi}(t), \int ACE_i(t), \Delta P_{windi}(t), \Delta P_{essi}(t), \Delta P_{evi}(t)\right\}$, which includes the essential state variables of LFC, i.e., frequency deviation, tie-line power, turbine-governor states, and the integral of ACE, as well as the power contributions from VPP components. $y_i(t) = ACE_i(t)$ and $w_i(t) = \Delta P_{di}(t)$,

$$A_{ii}=\begin{bmatrix} -\frac{D_i}{M_i} & -\frac{1}{M_i} & \frac{1}{M_i} & 0 & 0 & \frac{1}{M_i} & \frac{1}{M_i} & \frac{1}{M_i} \\ 2\pi \sum_{j=1,j\neq i}^{N} T_{ij} & 0 & 0 & 0 & 0 & 0 & 0 & 0 \\ 0 & 0 & -\frac{1}{T_{ch_i}} & \frac{1}{T_{ch_i}} & 0 & 0 & 0 & 0 \\ -\frac{1}{RT_{g_i}} & 0 & 0 & -\frac{1}{T_{g_i}} & 0 & 0 & 0 & 0 \\ \beta_i & 1 & 0 & 0 & 0 & 0 & 0 & 0 \\ 0 & 0 & 0 & 0 & 0 & \frac{k_{\beta_i}}{T_{windi}} & 0 & 0 \\ 0 & 0 & 0 & 0 & 0 & 0 & \frac{1}{T_{essi}} & 0 \\ 0 & 0 & 0 & 0 & 0 & 0 & 0 & \frac{1}{T_{evi}} \end{bmatrix},$$

$$A_{ij}=\begin{bmatrix} 0 & 0&0&0&0&0&0&0 \\ -2\pi T_{ij} & 0&0&0&0&0&0&0 \\ 0 & 0&0&0&0&0&0&0 \\ 0 & 0&0&0&0&0&0&0 \\ 0 & 0&0&0&0&0&0&0 \\ 0 & 0&0&0&0&0&0&0 \\ 0 & 0&0&0&0&0&0&0 \\ 0 & 0&0&0&0&0&0&0 \end{bmatrix}, F_i=\begin{bmatrix} -\frac{1}{M_i} \\ 0 \\ 0 \\ 0 \\ 0 \\ 0 \\ 0 \\ 0 \end{bmatrix},$$

$$B_i=\begin{bmatrix} 0&0&0&\frac{1}{T_{gi}}&0&0&0&0 \\ 0&0&0&0&0&\frac{k_{\beta i}}{T_{\text{windi}}}&0&0 \\ 0&0&0&0&0&0&\frac{1}{T_{\text{essi}}}&0 \\ 0&0&0&0&0&0&0&\frac{1}{T_{\text{evi}}} \end{bmatrix}^T, C_i=\begin{bmatrix} \beta_i \\ 1 \\ 0 \\ 0 \\ 0 \\ 0 \\ 0 \\ 0 \end{bmatrix}^T.$$

u_i in (5) represents the designed control input that satisfies

$$u_i(t)=-K_i y_i(t)-\sum_{j=i,j\neq i}^{n} K_{ij} y_j(t) \tag{6}$$

Remark 3. *In this study, VPPs serve as an aggregation entity for DERs encompassing wind power, ESSs, and EVs. The dynamic response characteristics of each individual resource are quantified by means of a first-order inertia model. These disparate resources are then consolidated into a single, cohesive controllable entity, which is subsequently incorporated into the global state-space representation of the multi-area LFC scheme. This integration empowers the aggregated resources to engage in power system frequency regulation through the utilization of AGC signals.*

Combining (5) and (6), we have

$$\begin{aligned} \dot{x}_i(t) =& A_{ii}x_i(t)+B_i\left(-K_i y_i(t)-\sum_{j=i,j\neq i}^{n} K_{ij}y_j(t)\right)+F_i w_i(t)+\sum_{j=1,j\neq i}^{n} A_{ij}x_j(t) \\ =& A_{ii}x_i(t)-B_iK_iy_i(t)-\sum_{j=i,j\neq i}^{n} B_iK_{ij}y_j(t)+F_iw_i(t)+\sum_{j=1,j\neq i}^{n} A_{ij}x_j(t) \\ =& A_{ii}x_i(t)-B_iK_iC_ix_i(t)-\sum_{j=i,j\neq i}^{n} B_iK_{ij}C_jx_j(t)+F_iw_i(t)+\sum_{j=1,j\neq i}^{n} A_{ij}x_j(t) \\ =& (A_{ii}-B_iK_iC_i)x_i(t)+\sum_{j=i,j\neq i}^{n}(A_{ij}-B_iK_{ij}C_j)x_j(t)+F_iw_i(t) \end{aligned} \tag{7}$$

Define $x(t)=col\{x_1(t),...,x_N(t)\}$, $y(t)=col\{y_1(t),...,y_N(t)\}$, $u(t)=col\{u_1(t),...,u_N(t)\}$, $w(t)=col\{w_1(t),...,w_N(t)\}$. The corresponding system model is given by:

$$\begin{cases} \dot{x}(t) = (A - BKC)\,x(t) + Fw(t) \\ y(t) = Cx(t) \end{cases} \tag{8}$$

where $A = \begin{pmatrix} A_{11} & A_{12} & \dots & A_{1N} \\ A_{21} & A_{22} & \dots & A_{2N} \\ \vdots & \vdots & \ddots & \vdots \\ A_{N1} & A_{N2} & \dots & A_{NN} \end{pmatrix}$, $K = \begin{pmatrix} K_1 & K_{12} & \dots & K_{1N} \\ K_{21} & K_2 & \dots & K_{2N} \\ \vdots & \vdots & \ddots & \vdots \\ K_{N1} & K_{N2} & \dots & K_N \end{pmatrix}$, $B = diag\{B_1, ..., B_N\}$, $C = diag\{C_1, ..., C_N\}$ and $F = diag\{F_1, ..., F_N\}$

The coexistence of DoS attacks and actuator failures is taken into account in this work.In particular, under DoS attacks, actuator may be unable to receive the control commands transmitted by the controller. According to [31], the DoS attack complies with the following mathematical model

$$Prob\{\alpha(t) = 1\} = \bar{\alpha} \tag{9}$$

$$Prob\{\alpha(t) = 0\} = 1 - \bar{\alpha} \tag{10}$$

where $0 < \bar{\alpha} \leq 1$, and $\alpha(t) = 0$ indicates that the control-actuator communication channel is blocked by a DoS attackand the control signal is completely interrupted, while $\alpha(t) = 1$ means the channel operates normally and the control signal can be successfully transmitted. Furthermore, to provide a more comprehensive and realistic analysis, actuator failures are also taken into consideration. Under such circumstances, the system input can be expressed as follows:

$$\tilde{u}(t) = \rho_i \alpha(t)\, u_i(t) \tag{11}$$

where $\underline{\rho}_i < \rho_i < \bar{\rho}_i$.

Considering the presence of DoS attacks and actuator failures, we can rewrite (8) in the following form:

$$\begin{cases} \dot{x}(t) = (A - \rho\alpha(t)\, BKC)\,x(t) + Fw(t) \\ y(t) = Cx(t) \end{cases} \tag{12}$$

where $\rho = diag\{\rho_1, \dots, \rho_N\}$

This study seeks to devise an appropriate feedback gain K, so that the stability of the closed-loop system given in (8) can be ensured in the presence of DoS attacks and actuator failures.

3 Main Results

In this section, system stability is investigated via the Lyapunov approach. It is shown that the closed-loop system remains boundedly stable despite the simultaneous existence of DoS attacks and actuator faults. Moreover, the corresponding feedback gain matrix is obtained by solving the matrix inequality given in (13).

Theorem 1. *The bounded stability of System (12) is guaranteed if there exist matrices P and $Y = KCP^{-1}$, as well as scalars δ_i and θ, such that*

$$\Psi = \begin{bmatrix} \Psi_{11} & P^{-1} \\ P^{-1} & -\theta I \end{bmatrix} < 0 \tag{13}$$

where $\Psi_{11} = AP^{-1} + P^{-1}A^T - 2\bar{\alpha}\underline{\rho}BY + \delta I$

Proof. To facilitate the subsequent analysis, the following Lyapunov function is introduced:

$$V(t) = x^T(t)\, Px(t) \tag{14}$$

Based on the system trajectory characterized by (12), the following can be derived:

$$\begin{aligned} & E\left\{\dot{V}(t)\right\} \\ & = 2E\left\{x^T(t) P\dot{x}(t)\right\} \\ & = 2x^T(t) P\left((A-\bar{\alpha}\rho BKC) x(t)+Fw(t)\right) \\ & = 2x^T(t)\left(PA-\bar{\alpha}P\rho BKC\right) x(t)+2x^T(t) PFw(t) \end{aligned} \tag{15}$$

A scalar δ can be determined such that

$$\begin{aligned} & 2x^T(t) PFw(t) \\ & \leq \delta x^T(t) PPx(t)+\frac{1}{\delta}\|F\|_F^2\|w(t)\|_2^2 \end{aligned} \tag{16}$$

Set $Y = KCP^{-1}$. With $\underline{\rho} = min\{\rho_1, ..., \rho_N\}$, the inequality $-\bar{\alpha}P\rho BKC < -\bar{\alpha}\underline{\rho}PBKC$ holds. We further have

$$\begin{aligned} & E\left\{\dot{V}(t)\right\} \\ & \leq x^T(t)\left(PA+A^TP-2\bar{\alpha}\underline{\rho}PBKC+\delta PP\right) x(t)+\frac{1}{\delta}\|F\|_F^2\|w(t)\|_2^2 \end{aligned} \tag{17}$$

By pre-multiplying inequality (13) with $\mathrm{diag}\{P, I\}$ and post-multiplying it by the transpose of this matrix, followed by the application of the Schur complement lemma, the following result can be derived:

$$PA+A^TP-2\bar{\alpha}\underline{\rho}PBKC+\delta PP<-\frac{1}{\theta}I \tag{18}$$

Based on (18), we have

$$\begin{aligned} & E\left\{\dot{V}(t)\right\} \\ & \leq -\frac{1}{\theta}\|x(t)\|_2^2+\frac{1}{\delta}\|F\|_F^2\|w(t)\|_2^2 \end{aligned} \tag{19}$$

When $x(t)$ is not contained within the region $\|x(t)\|_2^2 \leq \frac{\theta}{\delta}\|F\|_F^2\|w(t)\|_2^2$, it follows that $\mathbb{E}\left\{\dot{V}\right\} < 0$. This result indicates that the system described by (12) achieves bounded stability, which completes the proof.

□

Utilizing MATLAB to solve the LMI presented in (13), we obtain the associated matrix Y. By substituting the derived Y into the equation $Y = KCP^{-1}$, the corresponding feedback gain can be calculated.

4 ILLUSTRATIVE EXAMPLE

A simulation study is performed on a VPP-integrated two-area power system to verify the performance of the proposed control strategy, as depicted in Figure 2. All critical system parameters, sourced from [32], are presented in Tables 1 and 2.

Table 1. Parameters of power systems

Parameter	T_{ch}	T_g	R	D	β	M
Area 1	0.3	0.1	0.05	1.0	21.0	10
Area 2	0.4	0.17	0.05	1.5	21.5	12
$T_{12} = T_{21} = 0.1986$						

In the scenario where the system is free from DoS attacks and actuator failures, Load disturbances are set as $w_1(t) = w_2(t) = \frac{1}{200t}$. The initial state vectors are configured as $\bar{x}_1(0) = [0.2, 0.2, 0.5, 0.5, 0.2, 0.5, 0.5, 0.2]^T$ and $\bar{x}_2(0) = [0.5, 0.1, 0.5, 0.5, 0.2, 0.5, 0.5, 0.2]^T$. By solving inequality (13), the corresponding control gain can be obtained as follows:

$$K = \begin{bmatrix} -1.6248 & 3.0412 & 0.2296 & 0.0576 & 0.0545 & 0.0484 & 0.0213 & 0.0157 \\ -0.0904 & 0.3412 & -0.0093 & -0.0086 & -1.6138 & 3.3099 & 0.4232 & 0.1288 \end{bmatrix}^T.$$

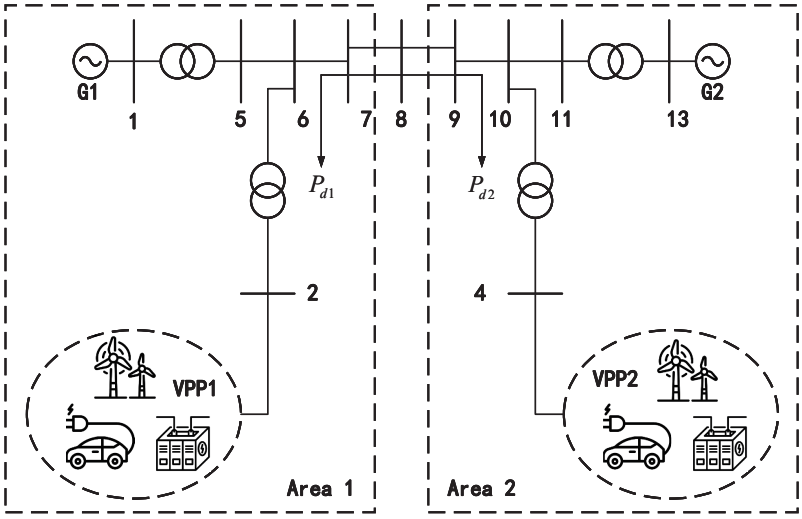

Figure 2. Architecture of a Two-Area Power System Integrated with VPPs.

Table 2. Parameters of VPPs

Parameter	T_{wind}	T_{ess}	T_{pv}
Area 1	1	0.1	0.05
Area 2	1.2	0.15	0.06

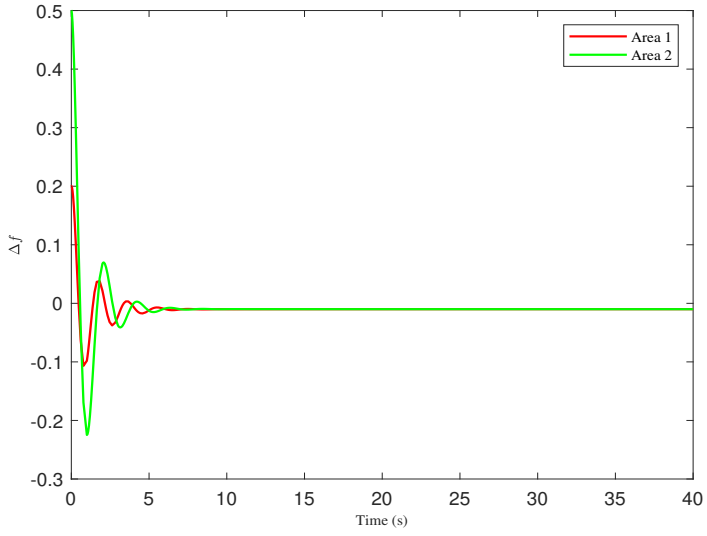

Figure 3. The trajectory of Δf when the system is free from DoS attacks and actuator failures

Simulation results are illustrated in Figures 3 and 4.

Figures 3 and 4 illustrate the dynamic trajectories of Δf and P_{tie} under the failure-free and attack-free scenario. The results demonstrate that the proposed control strategy can maintain the stable operation of the multi-area power system in the absence of DoS attacks and actuator failures.

In the scenario when the system is simultaneously subjected to both DoS attacks and actuator failures, we define $\bar{\alpha} = 0.9$, $\rho_1 = 0.9+0.1*cos(t)$ and $\rho_2 = 0.95+0.05*sin(t)$; accordingly, the lower bound $\underline{\rho} = 0.8$.

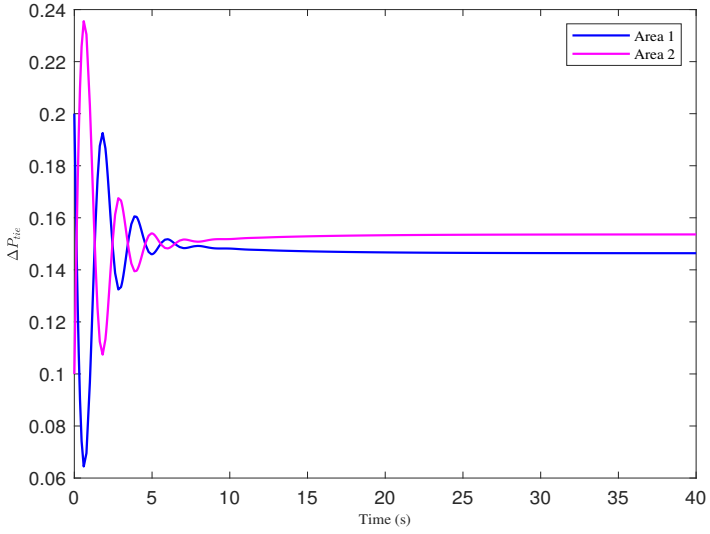

Figure 4. The trajectory of P_{tie} when the system is free from DoS attacks and actuator failures

Meanwhile, the load disturbance inputs are configured as $w_1(t) = w_2(t) = \frac{1}{200t}$, with the initial states assigned as $\bar{x}_1(0) = [0.2, 0.2, 0.5, 0.5, 0.2, 0.5, 0.5, 0.2]^T$ and $\bar{x}_2(0) = [0.5, 0.1, 0.5, 0.5, 0.2, 0.5, 0.5, 0.2]^T$. The required control gain is then obtained by solving inequality (13), as shown below:

$$K = \begin{bmatrix} -2.1970 & 3.5460 & 0.3178 & 0.0853 & -0.1415 & 0.2222 & 0.0561 & 0.0272 \\ -0.1034 & -0.2930 & -0.0271 & -0.0188 & -2.3286 & 4.8974 & 0.6322 & 0.1968 \end{bmatrix}^T$$

The corresponding simulation results are illustrated in Figures 5 and 6.

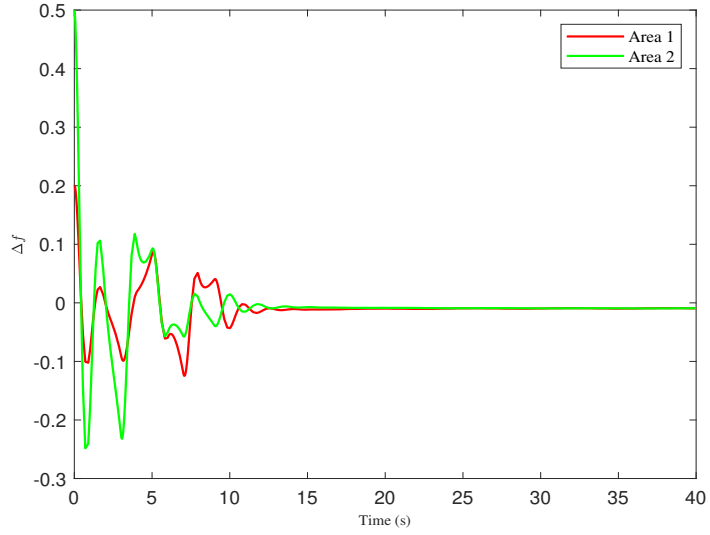

Figure 5. The trajectory of Δf when the system is subjected to DoS attacks ($\bar{\alpha} = 0.9$) and actuator failure.

Figures 5 and 6 present the dynamic trajectories of Δf and P_{tie} under the coexistence of DoS attacks and actuator failures. It can be observed from these figures that all trajectories eventually converge, which verifies the effectiveness of the proposed control strategy.

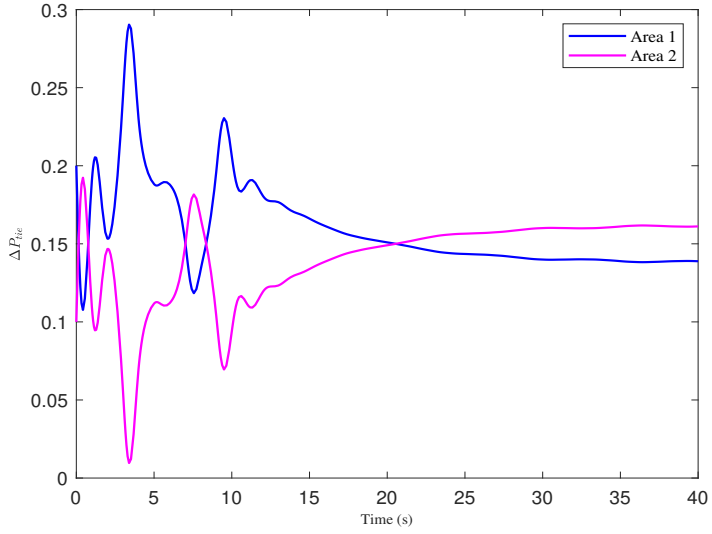

Figure 6. The trajectory of P_{tie} when the system is subjected to DoS attacks ($\bar{\alpha} = 0.9$) and actuator failures.

To further investigate the impact of DoS attack intensity, a comparative case is conducted by setting $\bar{\alpha} = 0.7$, representing a more severe communication disruption. The corresponding feedback gain matrix is re-calculated by solving the LMI in (13), as shown below:

$$K = \begin{bmatrix} -2.7528 & 4.8737 & 0.4279 & 0.1255 & -0.0161 & -0.1951 & -0.0303 & -0.0090 \\ -0.0171 & -0.0582 & -0.0149 & -0.0084 & -2.9738 & 5.7716 & 0.7050 & 0.1998 \end{bmatrix}^T.$$

The corresponding simulation results are depicted in Figs.7 and 8.

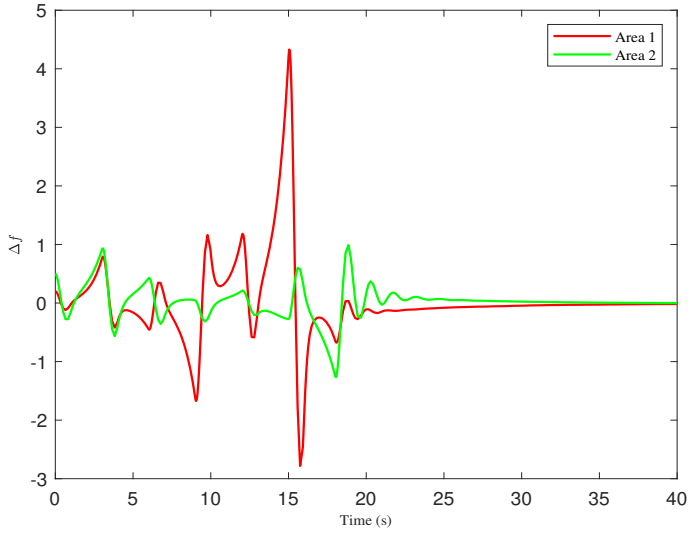

Figure 7. The trajectory of Δf when the system is subjected to DoS attacks ($\bar{\alpha} = 0.7$) and actuator failure.

Fig. 7 and 8 illustrates the system dynamic response under increased DoS attack intensity ($\bar{\alpha} = 0.7$). The results indicate that even when communication disruptions are significantly intensified, the proposed resilient control scheme effectively ensures system convergence.

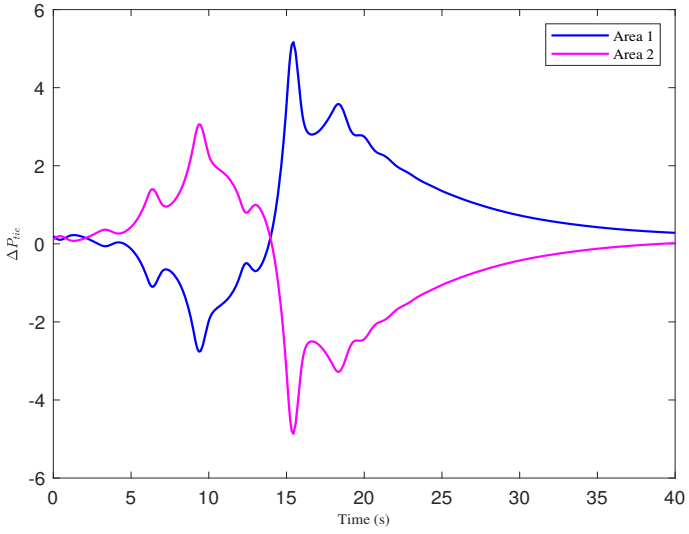

Figure 8. The trajectory of P_{tie} when the system is subjected to DoS attacks ($\bar{\alpha} = 0.7$) and actuator failures.

5 Conclusion

The LFC problem for multi-area power systems with integrated VPPs subject to DoS attacks and actuator failures is investigated in this paper. To tackle this challenge, a distributed control method utilizing both local and neighboring measurements is proposed. By constructing an appropriate Lyapunov function, a sufficient condition is derived to guarantee the bounded stability of the system, and the feedback gains are further obtained via the LMI technique. Finally, simulation results are provided to demonstrate the effectiveness and feasibility of the proposed control approach. In this study, attacks are only considered in the controller–actuator channel. In future work, we will extend the analysis to scenarios where attacks occur in multiple channels and investigate the corresponding resilient control strategies. In addition, communication delays will be incorporated into the system modeling framework.

Acknowledgments

We would like to express our sincere gratitude to all editors and reviewers for their invaluable assistance in improving this paper.

Funding

This work was supported in part by the National Natural Science Foundation of China under Grants U24A20268, 62373162

Conflicts of interest

The authors declare that they have no conflict of interest.

Data availability statement

The original data used in this study are available from the corresponding author upon reasonable request.

Author contribution statement

Yichao Wang wrote the original draft of the paper, developed the conceptualization, and completed the simulation experiments. Zhi-Wei Liu jointly wrote the paper and took charge of the paper revision.

References

[1] Pandey SK, Mohanty SR, Kishor N. A literature survey on load–frequency control for conventional and distribution generation power systems. Renew Sust Energ Rev. 2013; **25**: 318–334.
[2] Bevrani H. Robust Power System Frequency Control. Switzerland: Springer, 2014.
[3] Xie YJ, Zhang YC and Lee WJ et al. Virtual Power Plants for Grid Resilience: A Concise Overview of Research and Applications. IEEE/CAA J Automatica Sin 2024; **11**: 329–343.

[4] Zhang YF, Liu F and Wang ZJ et al. Robust Scheduling of Virtual Power Plant Under Exogenous and Endogenous Uncertainties. IEEE Trans Power Syst 2022; **37**: 1311–1325.
[5] Pourghaderi N, Fotuhi-Firuzabad M and Kabirifar M et al. Reliability-Based Optimal Bidding Strategy of a Technical Virtual Power Plant. IEEE Syst J 2022; **16**: 1080–1091.
[6] Toubeau JF, Nguyen TH and Khaloie H et al. Forecast-Driven Stochastic Scheduling of a Virtual Power Plant in Energy and Reserve Markets. IEEE Syst J 2022; **16**: 5212–5223.
[7] Ge CY, Lin SF and Li FX et al. Optimal Coordination Method for an ADN With Multiple Network-Constrained VPPs. IEEE Trans Power Syst 2025; **40**: 394–407.
[8] Bahloul M, Breathnach L, Khadem S. Residential Virtual Power Plant Control: A Novel Hierarchical Multi-Objective Optimization Approach. IEEE Trans Smart Grid 2025; **16**: 1301–1313.
[9] Oshnoei A, Kheradmandi M and Blaabjerg F et al. Coordinated control scheme for provision of frequency regulation service by virtual power plants. Appl Energy 2022; **325**: 119734.
[10] Gao S, Zhang H and Wang ZP et al. Optimal injection attack strategy for cyber-physical systems: a dynamic feedback approach. Secur Saf 2022; **1**: 2022005
[11] Liu J, Tang S Y and Gao S et al. Secure platooning control of connected vehicles against data injection attacks. Secur Saf 2025; **4**: 2025002.
[12] Sun J, Tan SW and Zheng HH et al. A DoS Attack-Resilient Grid Frequency Regulation Scheme via Adaptive V2G Capacity-Based Integral Sliding Mode Control. IEEE Trans Smart Grid 2023; **14**: 3046–3057.
[13] Zhang H, Chen Z and Yu C et al. Event-Trigger-Based Resilient Distributed Energy Management Against FDI and DoS Attack of Cyber–Physical System of Smart Grid. IEEE Trans Syst Man Cybern Syst 2024; **54**: 3220–3230.
[14] Chlela M, Mascarella D and Joós G et al. Fallback Control for Isochronous Energy Storage Systems in Autonomous Microgrids Under Denial-of-Service Cyber-Attacks. IEEE Trans Smart Grid 2018; **9**: 4702–4711.
[15] Chen W, Ding D and Dong H et al. Distributed Resilient Filtering for Power Systems Subject to Denial-of-Service Attacks. IEEE Trans Syst Man Cybern Syst 2019; **49**: 1688–1697.
[16] Ding L, Han QL and Ning B et al. Distributed Resilient Finite-Time Secondary Control for Heterogeneous Battery Energy Storage Systems Under Denial-of-Service Attacks. IEEE Trans Ind Informat 2020; **16**: 4909–4919.
[17] Lu KD, Zeng GQ and Luo X et al. An Adaptive Resilient Load Frequency Controller for Smart Grids With DoS Attacks. IEEE Trans Veh Technol 2020; **69**: 4689–4699.
[18] Wang J, Li Y and Wu Y et al. Fixed-Time Formation Control for Uncertain Nonlinear Multiagent Systems With Time-Varying Actuator Failures. IEEE Trans Fuzzy Syst 2024; **32**: 1965–1977.
[19] Wei L, Zhang Z. Adaptive compensation control of nonlinear systems with unknown actuator failures. Int J Robust Nonlinear Control 2023; **33**: 5645–5660.
[20] Ye D, Chen MM, Yang HJ. Distributed Adaptive Event-Triggered Fault-Tolerant Consensus of Multiagent Systems With General Linear Dynamics. IEEE Trans Cybern 2019; **49**: 757–767.
[21] Shen Q, Yue C and Goh CH et al. Active Fault-Tolerant Control System Design for Spacecraft Attitude Maneuvers with Actuator Saturation and Faults. IEEE Trans Ind Electron 2019; **66**: 3763–3772.
[22] Tariverdi A, Talebi HA, Shafiee M. Fault-tolerant consensus of nonlinear multi-agent systems with directed link failures, communication noise and actuator faults. Int J Control 2019; **94**: 60–74.
[23] Wen GG, Zhai XQ and Peng ZX et al. Fault-Tolerant secure consensus tracking of delayed nonlinear multi-agent systems with deception attacks and uncertain parameters via impulsive control. Commun Nonlinear Sci Numer Simul 2020; **82**: 105043.
[24] Hua YZ, Dong XW and Li QD et al. Distributed Fault-Tolerant Time-Varying Formation Control for Second-Order Multi-Agent Systems With Actuator Failures and Directed Topologies. IEEE Trans Circuits Syst II-Express Briefs 2018; **65**: 774–778.
[25] Rerkpreedapong D, Hasanovic A and Feliachi A et al. Robust load frequency control using genetic algorithms and linear matrix inequalities. IEEE Trans Power Syst 2003; **18**: 855-861.
[26] Luo HC, Hiskens IA and Hu ZC. Stability Analysis of Load Frequency Control Systems With Sampling and Transmission Delay. IEEE Trans Power Syst 2020; **35**: 3603-3615.
[27] Shangguan XC, Zhang CK and He Y et al. Robust Load Frequency Control for Power System Considering Transmission Delay and Sampling Period. IEEE Trans Ind Inform 2021; **17**: 5292–5303.
[28] Wang ZY, Wang Y and Xie L et al. Load Frequency Control of Multiarea Power Systems with Virtual Power Plants. Energies 2024; **17**: 3687.
[29] Wu J, Liu C, and Tao J et al. Hybrid Traffic Scheduling in 5G and Time-Sensitive Networking Integrated Networks for Communications of Virtual Power Plants. Appl Sci 2023; **13**: 7953.
[30] Cheng ZH, Hu SL, Yue D et al. Resilient Distributed Coordination Control of Multiarea Power Systems Under Hybrid Attacks. IEEE Trans Syst Man Cybern Syst 2022; **52**: 7-18.
[31] Liu K, Dong S, Liu M. Load Frequency Control of Networked Multi-Area Power Systems under DoS Attack and Actuator Failure. In: 2023 35th Chinese Control and Decision Conference (CCDC). IEEE, 2023: 1912–1915.
[32] Kang K, Shi N and Cai S et al. Distributed Model Predictive Load Frequency Control for Virtual Power Plants with Novel Event-Based Low-Delay Technique Under Cloud-Edge-Terminal Framework. Energies 2025; **18**: 1380.

Yichao Wang received the B.S. degree in automation from the China University of Geosciences, Wuhan, China, in 2022, and the M.Eng. degree in automation and control engineering from Northeastern University, Shenyang, China, in 2025. He is currently pursuing the Ph.D. degree in control science and engineering from the Huazhong University of Science and Technology, Wuhan, China. His current research interests include VPP, CPS and cybersecurity.

Zhi-Wei Liu received the B.S. degree in information management and information systems from Southwest Jiaotong University, Chengdu, China, in 2004, and the Ph.D. degree in control science and engineering from Huazhong University of Science and Technology, Wuhan, China, in 2011. He is currently a Professor with the School of Artificial Intelligence and Automation, Huazhong University of Science and Technology. His current research interests include cooperative control and optimization of distributed network systems